Suspended sediment flux at the Rhone river mouth (France) based on ADCP measurements during flood events.

Issa Sakho, Philippe Dussouillez, Doriane Delanghe, Boris Hanot, Guillaume Raccasi, Michal Tal, François Sabatier, Mireille Provansal, Olivier Radakovitch

Suspended sediment flux at the Rhone River mouth (France) based on ADCP measurements during flood events

Sakho, I.[a, b, c*], Dussouillez, P.[d], Delanghe, D.[d], Hanot, B.[d], Raccasi, G.[d], Tal, M [d], Sabatier, F. [d], Provansal, M. [d], Radakovitch, O. [d, e]

[a]. Département Sciences Expérimentales, UFR Sciences et Technologies, Université de Thiès, BP A 967, Thiès, Sénégal.
[b]. Laboratoire de Morphodynamique Continentale et Côtière, Université de Rouen Normandie, UMR CNRS 6143, 76 821 Mont-Saint Aignan, Cedex, France
[c]. Aix Marseille Univ, CNRS, IRD, Coll France, CEREGE, 13545 Aix-en-Provence, Cedex 04 France
[d]. Grontmij, 97 Rue De Freyr - Cs 36038, 34060 Montpellier Cedex 2, France
[e]. Institut de Radioprotection et de Sûreté Nucléaire (IRSN), BP 17, 92262 Fontenay-aux-Roses cedex, France

*. Corresponding authors.
E-mail : issa.sakho@gmail.com
olivier.radakovitch@irsn.fr

Abstract

Suspended sediment distribution and fluxes were estimated within the dominant channel at the mouth of the Rhone River for two annual flood events. The estimates were based on ADCP acoustic backscatter intensity and using calibration and post-processing methods to account for the grain-size distribution (GSDs). The fluxes were very similar to those obtained from suspended sediment measurements based on surface sampling at an automated station located 35 km upstream. Suspended Sediment Concentrations (SSC) and GSDs showed little variation along the channel cross section, except for a graduate suspension that appeared at the maximum of discharge, corresponding to velocities lower than 1 $m.s^{-1}$ near the bottom. However, without post processing to account for the GSD, an under-estimation of 10% was observed during the two floods periods. The two flood events, separated by only two weeks, had clear differences in suspended fluxes and SSC, with twice more flux during the first event.

Keywords: Suspended sediment flux, ADCP measurements, Backscatter calibration, Grain-

size distribution, flood events, Rhone River, France

1. Introduction

Determination of the quantity and quality (e.g., grain size, pollutants) of sediment delivered by rivers to the ocean is critical for managing and preserving deltas, shorelines, and marine ecosystems (Vörösmarty *et al.,* 2003; Limber *et al.,* 2008). Both the morphology of these systems and the habitat they support depend directly on the sediment flux delivered by the river, which itself depends on sediment production in the catchment (e.g. geology, precipitation, land use) and on the continuity of its transfer to the coast (e.g. retention dams, dredging; Blum *and* Tornqvist, 2000; Syvitski & Saito, 2003; Antonelli *et al.,* 2004; Provansal et al, 2014).

Suspended sediment fluxes (SSF) have been measured worldwide for a wide range of rivers (e.g. Walling *et al.,* 1992; Inman *and* Jenkins, 1999; Picouet *et al.,* 2001; Meybeck et al., 2003; Rovira *et al.,* 2005 ; Hu *et al.,* 2011 ; Boateng *et al.,* 2012 ; Unverricht *et al.,* 2014), and best practices for estimating these fluxes have been discussed by Moatar et al. (2006), Horowitz (2008) and Horowitz et al. (2015). The vast majority of these sediment flux estimates are based on suspended sediment concentrations (SSC) measured from a surface sample of the flow, and do not take into account variations in grain-size distributions and/or suspended sediment concentrations within the water column and the channel section.

Meybeck et al (2003) compiled a database of SSC and SSF measured in rivers worldwide and covering a range of flow regimes. According to their study, the difference in flux estimates from surface versus depth-integrated samples can induce one hundred percent variations in SSC, but they note that this range is negligible compared to the variation of up to six orders of magnitude due to temporal variation (e.g. discharge fluctuation). However, Horowitz (2008) demonstrated the marked spatial (vertical and lateral) and temporal variability in SSC in rivers for both constant and varying discharge and recommended that both depth and width-

integrated samples are needed to generate representative samples. Alternative methods that have been proposed and explored in order to measure SSC within the water column include measurements using an Optical Backscatter Sensor (Schoellhamer and Wright, 2013) and/or an Acoustic Doppler Current Profiler (ADCP, e.g. Tessier et al., 2008; Defendi et al., 2010 ; Duclos et al., 2013) – which was the focus of this study. However, as we will discuss in detail later, accurate estimates based on these techniques require analysis of water samples collected in real time in order to determine the grain size distribution (GSD) and calibrate its relationship with SSC.

The Rhone River, in the south of France, is the main source of freshwater and continentally derived sediments to the Mediterranean Sea. The downstream-most SSF has been monitored continuously since 2005 at the SORA monitoring station located in Arles (Figure 1a). These flux estimates are based on SSC measured from an automated surface flow sample collected once a day. While, this system provides an efficient and reliable method for obtaining a long and continuous record (Eyrolle et al 2012), it is not well suited for accurately estimating fluxes during floods, which can typically have strong vertical gradients in GSD and rapid changes in SSC. Furthermore, the system is susceptible to technical malfunctions when SSC is high, resulting in unreliable data. Annual SSF measured at Arles ranges between 1 and 11 $Mt.yr^{-1}$ (Pont *et al.,* 2002; Antonelli *et al.,* 2008; Ollivier et al 2011; Eyrolle *et al.,* 2012). The representativity of these SSC has been tested for discharges up to 3000 $m^3.s^{-1}$, but higher discharges could well induce more pronounced vertical stratification in SSCs and therefore larger errors in the estimation of SSF. Studies by Pont *et al.* (2002), Antonelli *et al.* (2008), Ollivier et al (2011), and Eyrolle *et al.,* (2012) estimate that between 80 - 90% of the Rhone annual suspended sediment flux is associated with floods. As such, there is a clear need for a more robust method to quantify SSF associated with these events. This study is part of an ongoing effort to develop a continuous monitoring system using an ADCP to estimate SSFs

84 during floods at the mouth of the Rhone delta. The study, spanning two flood events,
85 highlights the potential of this technique for characterizing spatial and temporal variability in
86 SSF and its relationship to flow hydrodynamics. The insights from this study provide an
87 important first step towards putting in place a fully autonomous system for continuous
88 monitoring of SSF on a large river. Our objective is to get a more precise estimate of sediment
89 delivery to the Rhone delta in order to better inform coastal management strategies. On the
90 long-term, we seek to relate SSF to discharge patterns and meteorological conditions in order
91 to identify the main sources of variability in flux delivered to the delta.

92 In this paper we present an analysis of ADCP measurements conducted during two
93 annual floods in 2012. XXXXX During both floods, we collected suspended sediment
94 samples at different locations and depths that provided precise information about SSC and
95 GSD. We used this data to calibrate the ADCP backscatter signal and compare flux estimates
96 with and without taking into account GSD. In addition, the samples provide a first glimpse at
97 how GSD distribution varies with depth over the course of annual floods on the Rhone River.

98 ## 2. Suspended Sediment Flux (SSF) estimates based on acoustic monitoring

99 Efforts to quantify SSF from the SSC distributions measured over the entire vertical
100 flow column and across an entire cross-section of channel have focused on the use of acoustic
101 Doppler Current Profilers (ADCPs; Alvarez and Jones, 2002; Gartner, 2004 ; Kostaschuk et
102 al., 2005; Tessier *et al.*, 2008; Ghaffari *et al.*, 2011; Duclos *et al.*, 2013). ADCPs use the
103 Doppler effect of sound scattered back from particles transported in suspension to measure
104 flow velocity. Holdaway *et al.* (1999) were amongst the first to demonstrate that this
105 backscatter signal could be also analyzed to extract information on SSC. Such acoustic
106 measurements have been used for example to study sedimentary processes in sandy systems
107 over short spatial and temporal scales such as tidal periods (Tessier *et al.*, 2008). Acoustic
108 Suspended Sediment Monitor is another system adapted for fine-grained cohesive sediment

and concentration ranging between 0.5 and 8 $g.l^{-1}$ (Shi, 2010).

Estimating solid flux from acoustic measurements requires calibrating the sound intensity scattered by particles in the flow with SSC. This is typically done by comparing the backscatter signal to measured SSC from samples collected at various depths in the water column and along a cross-section. Software for using this data to performing the calibration (e.g., Sediview, Plum Detection Toolbox) provide good results as long as data from direct measurements are available (Defendi *et al.,* 2010). However, a limitation of this technique is that the acoustic signal is grain-size dependent. In other words, for a given sediment concentration, the relative backscatter sensitivity can be different whether the GSD is coarser or finer, expressed in terms of relative percentages of clay, silt and sand (Guerrero *et al.,* 2011). The implication of this, is that flux estimates based on these calibrations are only accurate if the GSD remains constant over the range of flows that are monitored acoustically.

3. Description of the study site and ADCP monitoring

The Rhone River basin has an area of approximately 97,800 km^2 and drains several different mountain ranges including the Alps, the Jura, and the Cevennes. The mean annual flow discharge at the downstream is approximately 1700 $m^3.s^{-1}$, based on daily discharge records for the period 1920 – 2013 from the Beaucaire gauging station located 60 km upstream of the mouth (data available at http://hydro.eaufrance.fr). The Rhone is characterized by large inter-annual flow and sediment flux variability due to highly variable rainfall patterns and lithology within the catchment (Eyrolle-Boyer et al., 2012). This natural variability is enhanced by a series of hydroelectric dams (Provansal et al, 2014).

Approximately 50 km upstream of its mouth, the Rhone River separates into two branches – the Petit Rhone and the Grand Rhone (Figure 1a). The dominant branch (Grand Rhone) traverses the city of Arles and transports on average 90% of the flow (Boudet et al,

133 submitted). Annual floods in Arles have a discharge of approximately 3900 $m^3.s^{-1}$, and 2-yr
134 and 10-yr return period floods have discharges of 4800 and 7800 $m^3.s^{-1}$ respectively (Boudet
135 et al., submitted). Whatever is the peak discharge, flood durations range from 1 to 34 days
136 with a mean of 5 days (Eyrolle *et al.*, 2012; Boudet el al, submitted). About 90% percent of
137 the alluvial floor in our study area (see below) is covered by sand with a median grain size of
138 0.55-0.50 mm (Arnaud-Fassetta et al., 2003). This sand can be transported by suspension at
139 bankfull discharge (5400 $m^3.s^{-1}$) according to the Shields diagram (Arnaud-Fassetta et al.,
140 2003).

141 In order to improve estimates of total SSF delivered by the Rhone River to the
142 Mediterranean Sea, particularly by large and rapid floods, we equipped a passenger ferry,
143 known as Barcarin, which traverses the Grand Rhone 13 km upstream from the mouth (Fig 1)
144 with an ADCP in order to conduct continuous in-situ measurements.

145 The Barcarin ferry was equipped with an ADCP - RDI 600 kHz Workhorse Rio Grande
146 (Teledyne RD Instruments, 2007) set to operate with a 0.5 m vertical cell size. The ADCP was
147 mounted on the upstream side of the ferry and conducts measurements each time the ferry
148 crosses the river (Fig. 1b). The distance of the channel at this location is 350 m and it takes
149 the ferry approximately 3 minutes to traverse the full width (Fig. 1b). Approximately two
150 hundred crossings are made per day, resulting in an equivalent number of profiles acquired.
151 The ferry does not run between 2 AM and 4 AM and for discharges higher than 6000 $m^3.s^{-1}$.
152 The start and end of each profile are automatically determined from GPS positions of the
153 boat, with an error estimated at ±5m due to the width of the docks (Fig. 1b). This error is quite
154 large, sometimes leading successive crossings to be recorded as a single profile; these can be
155 manually separated later on. ADCP data are automatically transferred via Wifi to a computer
156 located in a building near the dock and from there to the CEREGE laboratory. The ADCP is
157 cleaned every few months of biofilm accumulations.

158 Other than short interruptions for technical maintenance and/or improvements, the
159 ADCP has been operating continuously since March 2012. A main advantage of this setup is
160 that the equipment is in place and fully operational when a flood arrives. This eliminates the
161 need of hastily organizing a monitoring trip (equipment and personnel) when flow levels start
162 to rise and ensures that sediment flux is monitored over the full duration of the flood. In
163 addition, the ferry's location, 32 km downstream of the SORA station (Fig. 1), permits
164 comparison between SSF estimates based on the ADCP and those estimated from surface
165 measurements at the station. Finally, as opposed to measurements collected at a single fixed
166 location, the ferry-mounted ADCP collects backscatter data along the full cross-section,
167 making it possible to study how suspended sediment is distributed both vertically and
168 horizontally.

169 **3.1 Measurements of in-situ suspended sediment concentrations and grain size**
170 **distributions**

171 The two annual events that we focus on in this paper occurred in 2012 on November
172 12th (hereafter referred to as the N-12 event) and on November 29th (N-29 event). These
173 events had a peak discharge of 4000 $m^3.s^{-1}$ and 4200 $m^3.s^{-1}$ respectively (Fig 2a). As was
174 previously mentioned, accurate estimation of SSCs from ADCP backscatter data requires a
175 GSD-based correction of the backscatter intensity with SSC calibration. In order to perform
176 this correction, we collected suspended sediment samples during the course of the two floods.
177 Figure 2a shows the hydrograph of these floods with black squares corresponding to the days
178 when in-situ samples were collected. The samples were collected from the ferry itself with a
179 5L horizontal (Niskin) sampling bottle. A multi-parameter probe (Diver CTD) was fixed to the
180 Niskin bottle in order to measure salinity, water temperature, and water depth for each sample.
181 Vertical samples were collected at three lateral locations: left and right banks and channel
182 center (Figure 2b) in order to characterize variations in sediment concentration. On each

183 location, six samples were collected between the surface of the flow and the channel bottom
184 (flow depths ranged from 7 to 10 m) with the exact depth of each sample recorded with the
185 probe.

186 Suspended sediment concentrations (SSC in $mg.l^{-1}$) were determined using a standard
187 filtration method (ISSeP, 2014): 500 ml filtered through 0.45 µm filters and dried at 40 °C for
188 48 h. One liter of sampled water was set aside for measuring GSD and stored at 4°C until it
189 could be analyzed (typically within a few days). The GSD were measured with a Beckman
190 Coulter LS 13 320 laser granulometer, with a range of 0.04–2000 microns in 117 fractions
191 collected on 132 detectors. The calculation model uses Fraunhöfer and Mie theory, water as
192 the medium (RI = 1.33 at 20°C), a refractive index in the range of that of kaolinite for the
193 solid phase (RI = 1.56), and absorption coefficients of 0.15 for the 780-nm laser wave length
194 and 0.2 for the polarized wavelengths. Ideally, a flow sample is poured all at once into the 1L
195 granulometer cup without the need for pre-treatment or sub-sampling. However, particle
196 concentrations during the floods were too high and exceeded the optimal obscuration
197 windows between 8 and 16% for diffraction and 50% and 70% for diffusion using the PIDS
198 technology (Polarization Intensity Differential Scattering). They were thus subsampled
199 through magnetic stirrer agitation before being injected into the granulometer. Six sub-
200 samples from a single bottle were measured to define the repeatability of the sub-sampling.
201 The two-sigma errors on the reproducibility were 1.5% on the mean and 0.2 % on the D_{50}
202 value. The validity of the analyses was also checked routinely using standard including G15
203 (D_{50}=15µm), SRM1003C (D_{50}=32µm) and SRM1004b (D_{50}=78.4µm). The ratio between
204 measured and certified values was respectively -2, +2 and -8% for these standards.

205 **3.2. Backscatter calibration**

206 Several methods have been proposed to calibrate the backscatter signal of an ADCP in
207 order to assess sediment flux in fluvial and estuarine environments. While we mention them

here, a detailed explanation of these methods is beyond the scope of this paper. Tessier *et al.* (2008) proposed a laboratory experiment calibration using optical backscatter sensor (OBS) turbidity measurement. Other researchers have used a post-processing method developed in Sediview (Land and Bray, 2000; Dredging Research Ltd., 2003; Cutroneo et al., 2012), which is based on a simplified version of acoustic theory in order to correct dispersion and attenuation of the acoustic backscatter signal (Defendi *et al.*, 2010). In this study we used the ViSea Plume Detection Toolbox (PDT) developed by Aqua Vision®. Like Sediview, this software uses acoustic theories to correct for signal losses associated with acoustic spreading, water absorption and particle attenuation (Francois & Garisson, 1982; Urick, 1983; Rijn, 1993). In the first phase of calibration, the default absorption coefficient of 0.181 $dB.m^{-1}$ for a 600 kHz ADCP frequency, which is estimated for a water temperature of 4°C and a salinity of 35 ppt, is corrected using field temperature and salinity measurements. Next, the absolute backscatter signal is converted to SSC based on direct measurements of SSC in $mg.l^{-1}$. The relationship between Absolute Backscatter (I) and SSC is defined by (*Visea PDT Manual*):

$$10 * \log(SSC) = 4.6 + 0.054 * I$$

Where SSC represent the Suspended Sediment Concentration (mg/l) and I the Absolute Backscatter Intensity.

Since absolute backscatter and therefore SSC depend on the degree of particle attenuation, the second step corrects for this by integrating the grain-size distribution. The ViSea PDT is not limited to only a single D_{50} value, offering the possibility of taking into account all size fractions ranging from sand (2000 µm) down to clay (0.24 µm). Finally, the software calculates a Total Suspended Sediment Flux ($kg.s^{-1}$) based on the backscatter signal calibration.

232 ## 4. Results

233 ### 4.1. Flow velocity and discharge

234 The structure and evolution of flow velocities across the transect during the N-12 event are
235 shown in figure 3a (mean velocities are indicated in each plot). Figure 3b shows that mean
236 flow velocities (calculated for ADCP profile per day) measured at Barcarin are well correlated
237 (R^2=0.97) with daily discharges measured upstream at the SORA station. The dataset spans a
238 large range of discharges during various days in 2012, for which the estimated mean
239 velocities varied between 0.18 and 1.4 $m.s^{-1}$. Maximum mean flow velocity (1.4 $m.s^{-1}$)
240 corresponded to the flood peaks of both the N-12 and N-29 events. During the flood peaks,
241 velocities were highest within the top 5 meters of the water column and decreased toward the
242 channel bottom and banks (Fig.3a).

243

244 ### 4.2. Suspended sediment concentrations and grain-size distributions from direct
245 sampling

246 Figure 4 shows the SSC measurements for the samples collected at different depths
247 and lateral positions within the channel. The different dates correspond to the black squares
248 shown in figure 2: 7 days and 6 days for the N-12 and N-29 events respectively. There was no
249 statistically significant difference in SSC with lateral position. The SSC was also uniform
250 with depth during low discharges and showed a slight increase with depth during the flood
251 peaks (right bank for the N-12 peak for example). The daily mean SSC (mean of all depths
252 and locations) ranged from a minimum of 40±4 $mg.l^{-1}$ on the 27th Nov to a maximum of
253 2853±140 $mg.l^{-1}$ on the 12th Nov, corresponding to the peak of the first flood. The mean SSC
254 was clearly lower for the second peak flood on the 29th Nov : 1100±180 $mg.l^{-1}$. To compare,
255 SSC values in the Grand Rhone typically ranged from 8 to 20 $mg.l^{-1}$ during usual flow
256 conditions.

257 Figure 5 shows the distribution of clay, silt, and sand as % of total sample volume for
258 samples collected at 0.5 m from the surface in the center of the channel. The GSD during the
259 N-12 and N-29 floods were very similar and consisted of the following clay-silt-sand
260 percentages respectively based on an average of all samples: 15-81-4 and 15-83-2 (Fig. 5).
261 For both floods, the range of percentage of clay-sized particles was between 11 – 22 % and
262 increased with increasing flow discharge, reaching a maximum value of 22% at the peak of
263 each flood (Fig. 5). Silt-sized particles represented the majority of the suspended sediment
264 load (around 80 %) and the sand fraction never exceeded 10 % (Fig. 5). This last fraction
265 increased during the two days following the N-12 peak.

266 **4.3. Backscatter signal calibration and GSD-based correction**

267 Calibration of the backscatter signal using the ViSea PDT® with SSC and GSD
268 resulted in linear regressions with R coefficients equal to 0.90 and 0.88 for the N-12 and N-29
269 floods respectively. We used these calibrations to estimate SSC from ADCP backscatter (using
270 the Plum Detection Toolbox) and then used these values to calculate a total SSF in $t.d^{-1}$ for
271 each sampling day.
272 Figure 6 illustrates the difference in SSC distributions estimated across the channel without
273 (Fig. 6a) and with (Fig. 6b) the correction for the GSD. This example corresponds to the N-12
274 event. When only measured SSC were considered in the calibration, the resulting estimate of
275 total SSF was 825 000 $t.d^{-1}$. When the calibration was based on both SSC and GSD, this total
276 SSF increased to 925 000 $t.d^{-1}$ (Fig. 7). For the N-29 event, the total SSF increased from
277 390200 to 431000 $t.d^{-1}$ with the correction. This discrepancy in the estimates of SSF
278 highlights the role that fine particles play in attenuating the acoustic signal, inducing here a
279 mean underestimation of about 10 %. During normal discharges, the homogeneity of GSD
280 does not influence so much the estimation of the total SSF.

281

282 **4.4. Estimated total suspended sediment flux**

283 Once we had estimated SSC from the calibrated ADCP signal (using both measured
284 SSC and GSD) corresponding to each of the samples that were collected, we proceeded to
285 estimate a daily SSF ($t.d^{-1}$) over the course of each flood event (Figures 7 and 8). For that, we
286 assumed that the concentrations estimated from the calibrated signals for one ADCP profile
287 were representative of the daily flux, and thus considered them to be uniform over a 24-h
288 period. We consider this a reasonable assumption since the variability of discharge within a
289 single day was low: the coefficient of variation for hourly discharge measured at SORA over
290 the span of a single day was between 1 and 9 %. The only exception was Nov. 27 when the
291 coefficient reached 22%. Furthermore, when we checked the backscatter profiles measured
292 one hour before and after the sampling, they were very similar to the profiles that were
293 calibrated. We thus assume that the maximum error associated with our daily SSF estimates is
294 ± 10-15 %.

295 Our estimates show that over the course of the N-12 flood, SSF increased from 69000
296 $t.d^{-1}$ during the two days prior to peak discharge to 925000 $t.d^{-1}$ at the flood peak (Fig. 7A-C)
297 then rapidly decreased to 123000 $t.d^{-1}$ and 6700 $t.d^{-1}$ for 2 and 7 days post-peak respectively
298 (fig 7 E-G). Maximum daily SSF corresponded to maximum discharge (Fig. 7H). A strong
299 vertical gradient in SSC can be seen on the 11^{th} and 12^{th} of November – immediately ahead of
300 and during the maximum discharge (Fig. 7 B-C). This maximum vertical gradient did not
301 coincide with the increase in the sand fraction shown in figure 4. SSC was approximately
302 3000 $mg.l^{-1}$ near the channel bottom and decreased to 2500 $mg.l^{-1}$ at 4 m below the surface.
303 SSC once again became uniform when discharge decreased, stabilizing at a value of
304 approximately 700 $mg.l^{-1}$ (Fig. 7E). As discharge decreased during the falling limb of the
305 hydrograph, SSC were high compared to similar discharges during the rising limb. This trend
306 is typical of leading hysteresis in sediment transport during floods and is generally associated

307 with resuspension of sediments from the bed (Horowitz 2008). Similar trends are observed for
308 the N-29 flood, although vertical gradients in SSC were limited to one day (Fig. 8C&F). As
309 mentioned earlier, total SSF was twice as high during the N-12 event as in the N-29 event
310 despite similar daily peak discharges (Fig. 2a).
311
312 **5. Discussion**
313 Estimates of SSC and SSF from ADCP measurements conducted over the course of two
314 flood events from the Barcarin ferry near the mouth of the Rhone River showed good
315 correlation with their respective flood hydrographs (Fig. 7H & Fig. 8F). Furthermore, the SSF
316 estimates are very similar to those obtained from the automated sampling station SORA
317 located 32 km upstream (Fig. 9). This comparison shows a strong linear relationship ($y = 0.6803x + 67067$; $R^2 = 0.6$, $n=12$; $p>0,05$, not shown), a relation further improved ($y = 0.8719x + 26252$; $R^2 = 0.9$; $p>0,001$) when we correct for the time-lag between the two
320 locations (approximately 10 h for a mean flow velocity = 1 $m.s^{-1}$). This strong relationship is
321 likely due to the fact that the vertical gradient in SSC was weak for the two monitored floods
322 (fig 3), and confirms that surface samples at SORA are representative of SSC over the entire
323 vertical flow column for annual return floods, such as the two events monitored here. It
324 remains unknown how SSC is distributed vertically for larger floods, but our data indicate that
325 a suspended gradient may develop at higher discharges. This in agreement with Arnaud-
326 Fassetta et al (2003) who shown that Shields diagram indicates that transport of sand can be
327 common (and in suspension) at bankfull discharge (5400 $m^3.s^{-1}$, higher than our peak
328 discharges).
329 The two consecutive floods had very similar peak discharges and hydrograph shapes,
330 but estimates of daily SSF were twice as high in the first event. This difference does not
331 appear to be related to the relative contributions of different tributaries during each event.

Indeed, the major tributaries of the Rhone contributed in a similar manner to the total discharge during both events as follows: 10-15% from the Durance, 15-20% from the Isere, 25-30% from the Saone and 40% from the Rhone upstream of Lyon (estimates are based on daily discharges reported at http://hydro.eaufrance.fr). Therefore, the difference in SSC is likely explained by a difference in the amount of material eroded in the tributary basins and the channel banks, and/or a decrease of sediment available for resuspension from the riverbed between the first and second flood. Zebracki et al (2015) have demonstrated the role of remobilized sediment as a significant secondary source, based on a fingerprinting approach using plutonium activity ratios associated with particles.

The estimated total solid flux transported during these two events (8 days in total) was 2.7 10^6 tons. This value represents 50 % of the annual SSF in 2012 (5.6 10^6 tons) estimated from measurements at the SORA station (unpublished data, SORA station database). In addition to the November floods, high discharges occurred in January and December 2012 (average daily discharges were between 2900 to 3800 $m^3.s^{-1}$ from January 2 – 10, and 3100 to 3600 $m^3.s^{-1}$ from December 16 – 30.). The cumulative total SSF transported by these four events represents 82 % of the annual suspended sediment flux, a typical value for the flux transported by annual floods in the Rhone (Eyrolle et al, 2012).

A synthesis of SSF transported by the floods since 2005 based on data from SORA station showed that fluxes are influenced by factors other than maximum discharge such as location of precipitation in the catchment area and sometimes dam management (Eyrolle et al, 2012). The results of this study support these observations and highlight the role of sediment available for resuspension in the riverbed, as well as the role of antecedent conditions (i.e. flood succession). Continuous monitoring is therefore necessary to accurately quantify long-term trends and to estimate SSF contributions from individual events. In addition to informing coastal management, this type of data is important to constrain the flux of various

hydrophobic pollutants including metals, PCBs and other organic contaminants (Ollivier et al., 2011).

Conclusion

a. In this study we used the Plum Detection Toolbox to calibrate suspended sediment concentrations (SSC) from ADCP acoustic backscatter and used this to estimate suspended sediment flux for two annual floods on the lower Rhone River.

b. The ADCP in this study was mounted on a ferryboat that traverses the dominant branch of lower Rhone River (Grand Rhone) multiple times a day. This setup has enabled continuous acquisition for more than 4 years up to now and ensures that the equipment is in place when a flood arrives.

c. We showed that ADCP backscatter provides a viable method for estimating SSC during floods when the signal is properly calibrated using SSC and Grain-Size Distribution (GSD) data from measured samples. Our results show that vertical SSC distributed over the river section is necessary to obtain a good calibration of the backscatter signal. When GSD was not accounted for, Suspended Sediment Flux (SSF) was underestimated by 10% (Fig. 2b).

d. ADCP allows to understand the structure of the solid flow throughout the channel section and to better assess SSF, particularly during flood events.

e. Suspended sediment for the two floods investigated was dominated by silts and clays which have an effect on the acoustic signal in water.

f. Analysis of the sediment transported in suspension from samples collected at different vertical depths showed uniform concentrations and GSD with depth. A vertical gradient was visible only at peak discharge.

g. Estimates of SSF based on ADCP data were similar to those based on surface samples collected at the automatic SORA station, located 32 km upstream. This similarity is linked to the weak vertical gradient in SSC for the two floods.

h. The two flood events analyzed for this study, separated by only a few days, showed clear differences in suspended SSC and SSF, with twice more suspended sediment transported during the first event. We attributed this decrease to the amount of sediment available from hillslope and bank erosion or more probably from resuspension within the riverbed. These differences in fluxes for similar magnitude events highlight the difficulty in estimating sediment fluxes precisely in the absence of continuous measurements.

Acknowledgements

This work was funded by the Regional Council of Bouches-du-Rhone and Rhone Sediment Observatory which is funded by the CNR, EDF, Agence de l'Eau RMC and PACA, Rhone and Languedoc-Roussillon regional councils. We are very grateful to help from the Syndicat Mixte d'Aménagement des Digues du Delta du Rhône et de la Mer.

References

Alvarez, L.G., Jones, S.E., 2002. Factors influencing suspended sediment flux in the Upper Gulf of California. Estuarine, Coastal and Shelf Science 54, 747-759 p.

Antonelli, C., Eyrolle, F., Rolland, B., Provansal, M., Sabatier, F., 2008. Suspended sediment and 137Cs fluxes during the exceptional December 2003 flood in the Rhone River, southeast France. Geomorphology 95, 350-360 p.

Antonelli, C., Provansal, M., Vella, C., 2004. Recent morphological changes of a channel in deltaïc environment. The case of the Rhône River, France. Geomorphology 57, 385-402.

Arnaud-Fassetta, G., Quisserne, D., Antonelli, C. 2003. Downstream grain-size distribution of

403 surficial bed material and its hydro-geomorphological significance in a large and
404 regulated river: the Rhône River in its delta area (France). Géomorphologie, 9, 33-49.
405 Blum, M., Tornqvist, T.E., 2000. Fluvial response to climate and sea-level changes: a review
406 and lookforward. Sedimentology 47, 2-48.
407 Boateng, I., Bray, M., Hooke, J. 2012. Estimating the fluvial sediment input to the coastal
408 sediment budget: A case study of Ghana. Geomorphology 138, 100-110.
409 Boudet L., Sabatier F., Radakovitch O. In press. Modelling of sediment transport pattern in
410 the mouth of the Rhone delta: role of storm and flood events. *Estuarine, Coastal and*
411 *Shelf Science.*
412 Bravard, J.P., Petit, F., 1997. Les cours d'eau. Dynamique du système fluvial. Armand
413 Colin/Masson, Paris.
414 Cutroneo L., Castellano M., Pieracci A., Povero P., Tucci S., Capello M. 2012. The use of a
415 combined monitoring system for following a turbid plume generated by dredging
416 activity in a port. Journ. Soil Sed. 12, 797-809.
417 Defendi, V., Kovačević, V., Arena, F., Zaggia, L. 2010. Estimating sediment transport from
418 acoustic measurements in the Venice Lagoon inlets. Continental Shelf Research 30,
419 883-893 p.
420 Dredging Research Ltd., 2003. The Sediview Method. Sediview Procedure Manual, DRL
421 Software Ltd., Godalming, UK, 83pp.
422 Duclos, P.A., Lafite, R., Le Bot, S., Rivoalen, F., Cuvillier, A. 2013. Dynamics of Turbid
423 Plumes Generated by Marine Aggregate Dredging: An Example of a Macrotidal
424 Environment (the Bay of Seine, France). Journal of Coastal Research, 29 (6a), 25-37 p.
425 Eyrolle, F., Charmasson, S., Louvat, D., 2004. Plutonium isotopes in the lower reaches of the
426 River Rhône over the period 1945–2000: fluxes towards the Mediterranean Sea and
427 sedimentary inventories. J. Environ. Radioact. 74, 127–138.

428 Eyrolle, F., Radakovitch O., Raimbault P., Charmasson S., Antonelli C., Ferrand E., Aubert
429 D., Raccasi G., Jacquet S., Gurriaran R. 2012. Consequences of hydrological events on
430 the delivery of suspended sediment and associated radionuclides from the Rhône River
431 to the Mediterranean Sea. *J. Soils Sediments* **12,** 1479–1495

432 Ferré, B., Guizien, K., Durrieu de Madron, X., Palanques, A., Guillén, J., Grémare, A., 2005.
433 Fine-grained sediment dynamics during a strong storm event in the inner-shelf of the
434 Gulf of Lion (NW Mediterranean), Cont. Shelf Res. 25 (19–20), 2410-2427.

435 Francois, R.E., Garrison, G.R., 1982. Sound absorption based upon ocean measurement, part
436 II, J. Acoust. Soc. Am. 72 (6), 1870-1890.

437 Gartner, J.W., 2004. Estimating suspended solids concentrations from backscatter intensity
438 measured by acoustic Doppler current profiler in San Francisco Bay, California. Marine
439 Geology 211, 169-187 p.

440 Ghaffari, P., Azizpour, J., Noranian, M., Chegini, V., Tavakoli, V., Shah-Hosseini, M. 2011.
441 Estimating suspended sediment concentrations using a broadband ADCP in Mahshahr
442 tidal channel. Ocean Sci. Discuss., 8, 1601-1630.

443 Guerrero M., Szupiany R.N., Amsler M. 2011. Comparison of acoustic backscaterring
444 techniques for suspended sediment investigations. Flow measurement and
445 instrumentation. 22, 392-401.

446 Holdaway, G.P., Thorne, P.D., Flatt, D., Jones, S.E., Prandle, D. 1999. Comparison between
447 ADCP and transmissometer measurements of suspended sediment concentration, Cont.
448 Shelf Res., 19 (3), 421-441.

449 Hoitink, A.J.F., Hoekstra, P. 2005. Observations of suspended sediment from ADCP and OBS
450 measurements in a mud-dominated environment. Coastal Engineering 52, 103-118.

451 Horowitz, A.J., Clarke, R.T., Merten, G.H. 2015. The effects of sample scheduling and sample
452 numbers on estimates of the annual fluxes of suspended sediment in fluvial systems.

453 Hydrological Processes, 29, 531-543.

454 Horowitz, A. J. 2008. Determining annual suspended sediment and sediment-associated trace
455 element and nutrient fluxes. *Sci. Total Environ.* 400, 315–43.

456 Hu, J., Pan, J., Guo, X., Zheng, Q. 2011. A summary of special section: regional
457 environmental oceanography in the South China Sea and its adjacent areas (REO-SCS).
458 *J. Oceanography* 67, 675-676.

459 Inman, D.L., Jenkins, S.A., 1999. Climate change and the episodicity of sediment flux of
460 small California Rivers. *Journal of Geology* 107, 251-270.

461 Kostaschuk, R., Best, J., Villard, P., Peakall, J., Franklin, M., 2005. Measuring flow velocity
462 and sediment transport with an acoustic Doppler current profiler. *Geomorphology* 68,
463 25-37.

464 Land, J.M., Bray, R.N., 2000. Acoustic measurement of suspended solids for monitoring of
465 dredging and dredged material disposal. Journal of Dredging Engineering 2 (3), 1–17.

466 Limber, P.W., Patsch, K.B., Griggs, G.B., 2008. Coastal sediment budgets and the littoral
467 cutoff diameter: a grain size threshold for quantifying active sediment inputs. *Journal of*
468 *Coastal Research* 24, 122-133.

469 Meybeck, M., Laroche, L., Dürr, H., Syvitski, J. P. 2003. Global variability of daily total
470 suspended solids and their fluxes in rivers. *Glob. Planet. Change* **39,** 65–93.

471 Ollivier P., Radakovitch O., Hamelin B. (2011) Major and trace partition and fluxes in the
472 Rhone river. *Chem. Geol..285, 1-4; 15-31.*

473 Moatar F., Person G., Meybeck M., Coynel A., Etcheber H., Crouzet, P. 2006. The influence
474 of contrasting suspended particulate matter transport regimes on the bias and precision
475 of flux estimates. Science of the Total Environment, 370, 515-531.

476 Picouet, C., Hingray, B., Olivry, J.C., 2001. Empirical and conceptual modelling of the
477 suspended sediment dynamics in a large tropical African river: the Upper Niger river

basin. J. Hydrol. 250, 19-39 p.

Provansal M., Dufour S., Sabatier F., Antony E., Raccasi G., Robresco S. 2014. The geomphic evolution and sediment balance of the lower Rhone River (southern France) over the last 130 years: hydropower dams versus other control factors. *Geomorphology*. 219, 27-41.

Pont, D., Simonnet, J.P., Walter, A.V., 2002. Medium-term changes in suspended sediment delivery to the ocean: consequences of catchment heterogeneity and river management (Rhône River, France). *Estuar. Coast. Shelf Sci.* 54, 1–18.

Rijn, V. 1993. Principles of Sediment Transport in Rivers, Estuaries and Coastal Seas. Amsterdam: Aqua Publications, ISBN 90-800356-2-9 bound NUGI 816/831, 690 p.

Rovira, A., Batalla, R.J., Sala, M. 2005. Fluvial sediment budget of a Mediterranean river: the lower Tordera (Catalan Coastal Ranges, NE Spain). *Catena* 60, 19-42.

Sabatier, F., Maillet, G., Provansal, M., Fleury, T.J., Suanez, S., Vella, C. 2006. Sediment budget of the Rhône delta shoreface since the middle of the 19th century. *Marine Geology* 234, 143-157.

Schoellhamer, D.H., Wright A.S. 2003. Continuous measurement of suspended-sediment discharge in rivers by use of optical backscatterance sensors. Erosion and Sediment Transport Measurement in Rivers: Technological and Methodological Advances 1 (Proceedings of the Oslo Workshop, June 2002). IAHS Publ. 283.

Shi, Z., 2010. Tidal resuspension and transport processes of fine sediment within the river plume in the partially-mixed Changjiang estuary, China: a personal perspective, *Geomorphology.* 121, 133-151.

Syvitski J., Saito Y. 2007. Morphodynamics of deltas under the influence of humans. *Global Planet. Change*. 57, 3-4, 261-282.

Teledyne, RD Instruments, 2007. WorkHorse Rio Grande Acoustic Doppler Current Profiler.

503 Technical Manual P/N 957-6241-00, Teledyne RD Instruments, Poway, CA, 254pp.
504 Tessier, C., Le Hir, P., Lurton, X., Castaing, P. 2008. Estimation de la matière en suspension à
505 partir de l'intensité rétrodiffusée des courantomètres acoustiques à effet Doppler
506 (ADCP). *Comp. Rendu Geoscience* 340, 57-67.
507 Unverricht, D., Nguyen, T.C, Heinrich, C., Szczuciński, W., Lahajnar, N., Stattegger, K. 2014.
508 Suspended sediment dynamics during the inter-monsoon season in the subaqueous
509 Mekong Delta and adjacent shelf, southern Vietnam. *Journal of Asian Earth Sciences*
510 79, Part A, 509-519.
511 Urick, R.J., 1983. Principles of Underwater Sound. McGraw-Hill Book.
512 Vörösmarty, C., Meybeck, M., Fekete, B., Sharma, K., Green, P., Syvitski, J.P.M., 2003.
513 Anthropogenic sediment retention: major global-scale impact from the population of
514 registered impoundments. *Global and Planetary Change* 39, 169-190.
515 Wall, G.R., Nystrom, E.A., Litten, S., 2008. Suspended sediment transport in the freshwater
516 reach of the Hudson River estuary in eastern New York. Estuaries & Coasts. 31, 542-
517 553.
518 Walling, D.E., Webb, D.W., Woodward, J.C., 1992. Some sampling considerations in the
519 design of effective strategies for monitoring sediment-associated transport. IAHS Publ.
520 210, 279–288.
521
522 Zebracki M., Eyrolle-Boyer F., Evrard O., Claval D., Mourier B., Gairoard S., Cagant X.,
523 Antonelli C. 2015. Tracing the origin of suspended sediment in a large Mediterranean
524 river by combining continuous river monitoring and measurement of artificial and
525 natural radionuclides. *Science of the Total Environment.* 502, 122-132.
526
527
528 **CAPTIONS**
529

Figure 1. a). The Rhone River Delta highlighting the location of the Barcarin ferry crossing on the Grand Rhone and the city of Arles where the SORA station is located. **b)** An aerial photo of the Barcarin ferry landing. The white dotted line shows the average trajectory of the ferry between the right and left banks of the Grand Rhone. The white dots mark the locations where the ADCP measurements automatically start and stop.

Figure 2. a) Mean daily discharge ($m^3.s^{-1}$) of the Rhone river for the month of November, 2012 highlighting the two annual events N-12 (12^{th} Nov.) and N-29 (29^{th} Nov) that were monitored in this study. The black squares indicate the days on which the flow was sampled. Discharge measurements were conducted at the SORA station in Arles (32km upstream) and provided by the CNR. **b)** a cross-sectional view of the channel showing in red the locations where samples were collected at different depths in the water column.

Figure 3. a) Distribution of flow velocities measured with the Barcarin ferry ADCP during the N-12 flood. The date and mean current speed are indicated in each panel**. b).** Relationship between mean Barcarin ADCP flow velocities and corresponding discharge measured at the SORA station at Arles.

Figure 4. Suspended sediment concentrations ($mg.l^{-1}$) with depth at the three sampling locations (left and right banks and middle channel) for the N-12 (black) and N-29 (white) floods. The legend refers to the sampling date, and the measurements associated with each flood peak are highlighted.

Figure 5. The relative grain-size fractions: clay, silt, and sand, for each of the suspended samples collected at 0.5 m from the surface of the flow throughout the two monitored floods. During the two flood events, there are no daily vertical variation of sediment grain size.

Figure 6. An example of SSC distribution along the cross section based on ADCP backscatter calibrated **(a)** without accounting for GSD and **(b)** with GSD correction included.

Figure 7. A – G) Suspended sediment flux based on corrected ADCP measurements across the river for the N-12 flood. The date and total flux ($t.d^{-1}$) are indicated in each panel. H) Mean daily discharge measured at Barcarin and mean daily suspended sediment flux estimated from ADCP measurements for the N-12 flood.

Figure 8. A – Z) Suspended sediment flux based on corrected ADCP measurements across the river for the N-29 flood. The date and total flux ($t.d^{-1}$) are indicated in each panel. H) Mean daily discharge at Barcarin and mean daily suspended sediment flux estimated from ADCP measurements for the N-29 flood.

Figure 9. Comparison of suspended sediment flux (tons/day) during the rising and falling limbs of the 2 monitored floods (N-12 and N-29) based on measurements from automated surface samples at the SORA station in Arles and calibrated ADCP backscatter at the Barcarin crossing.

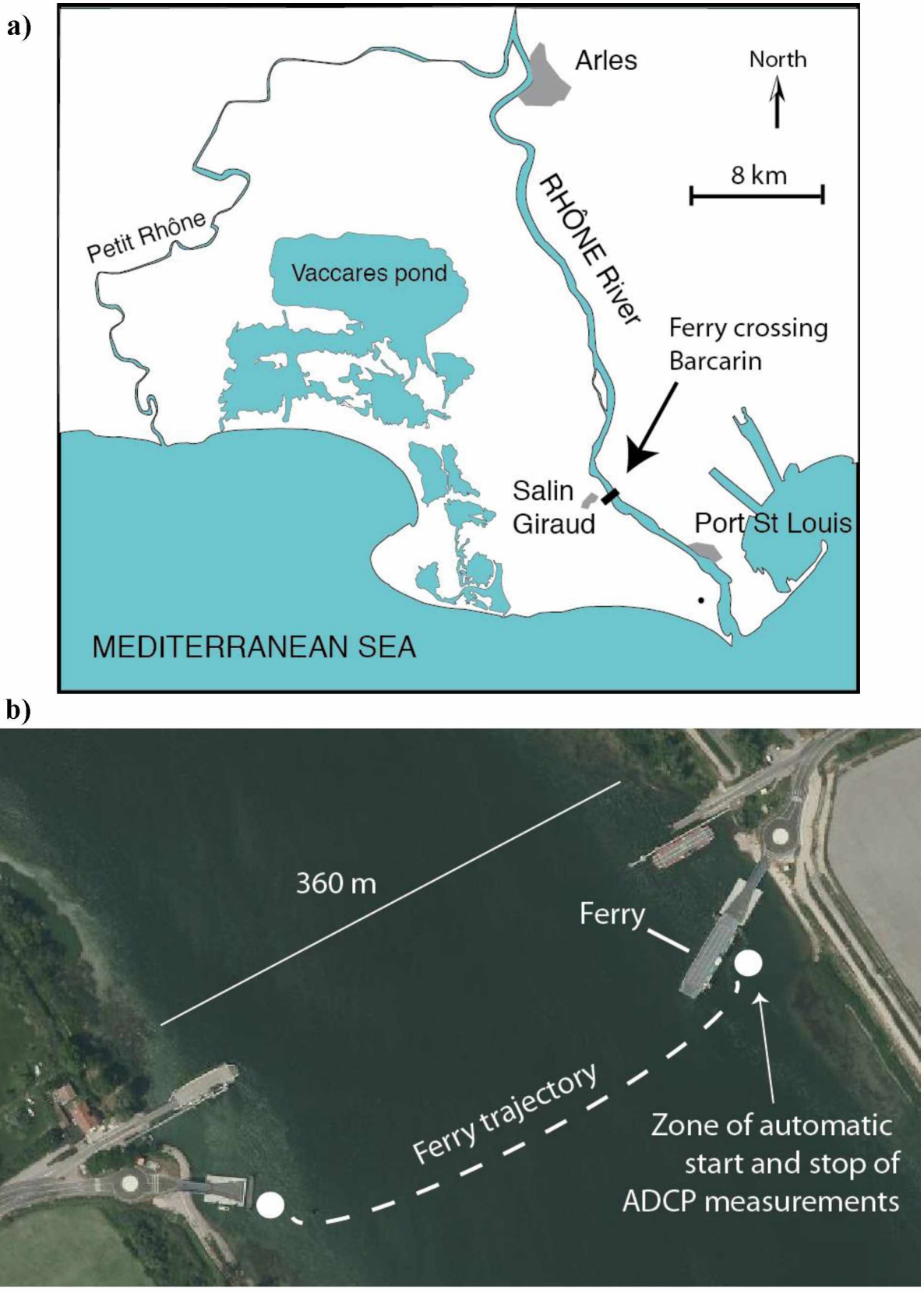
a)
Arles
North
8 km
Petit Rhône
RHÔNE River
Vaccares pond
Ferry crossing
Barcarin
Salin
Giraud
Port St Louis
MEDITERRANEAN SEA
b)
360 m
Ferry
Ferry trajectory
Zone of automatic
start and stop of
ADCP measurements

Figure 1.

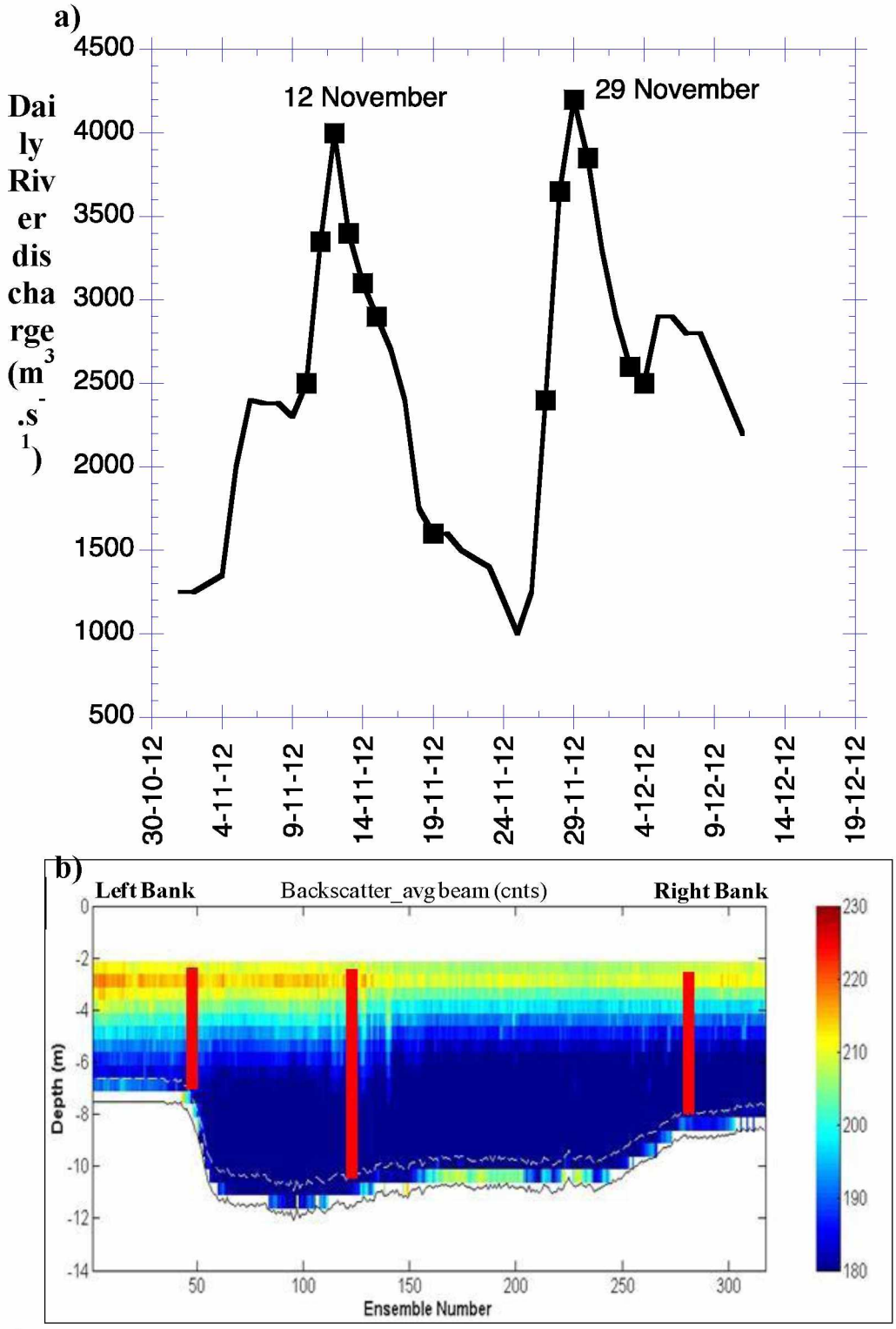
a)
Daily River discharge (m3.s-1)
12 November
29 November
4500
4000
3500
3000
2500
2000
1500
1000
500
30-10-12
4-11-12
9-11-12
14-11-12
19-11-12
24-11-12
29-11-12
4-12-12
9-12-12
14-12-12
19-12-12
b)
Left Bank
Backscatter_avg beam (cnts)
Right Bank
Depth (m)
0
-2
-4
-6
-8
-10
-12
-14
50
100
150
200
250
300
Ensemble Number
230
220
210
200
190
180

Figure 2.

a)

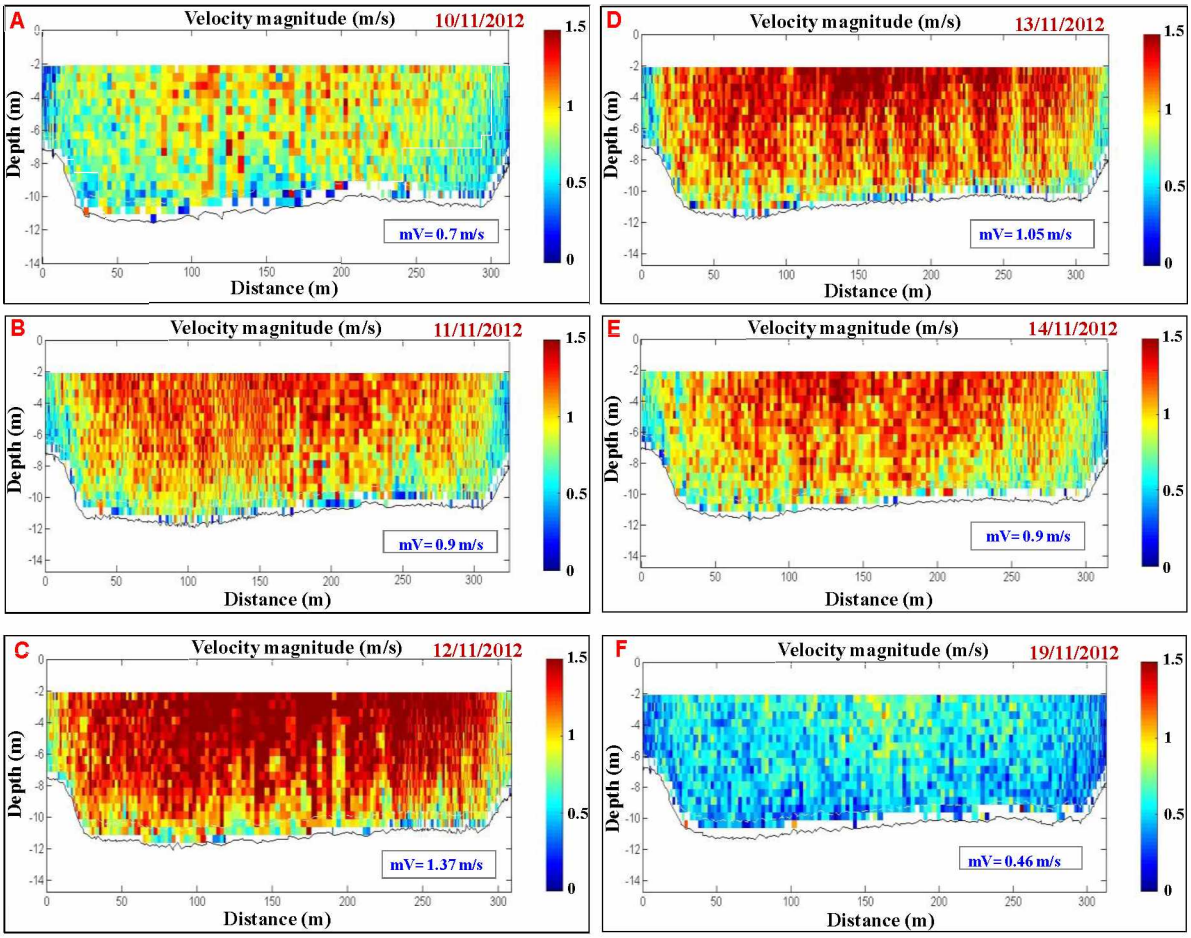
A
Velocity magnitude (m/s)
10/11/2012
mV= 0.7 m/s
D
Velocity magnitude (m/s)
13/11/2012
mV= 1.05 m/s
B
Velocity magnitude (m/s)
11/11/2012
mV= 0.9 m/s
E
Velocity magnitude (m/s)
14/11/2012
mV= 0.9 m/s
C
Velocity magnitude (m/s)
12/11/2012
mV= 1.37 m/s
F
Velocity magnitude (m/s)
19/11/2012
mV= 0.46 m/s
Depth (m)
Distance (m)

b)

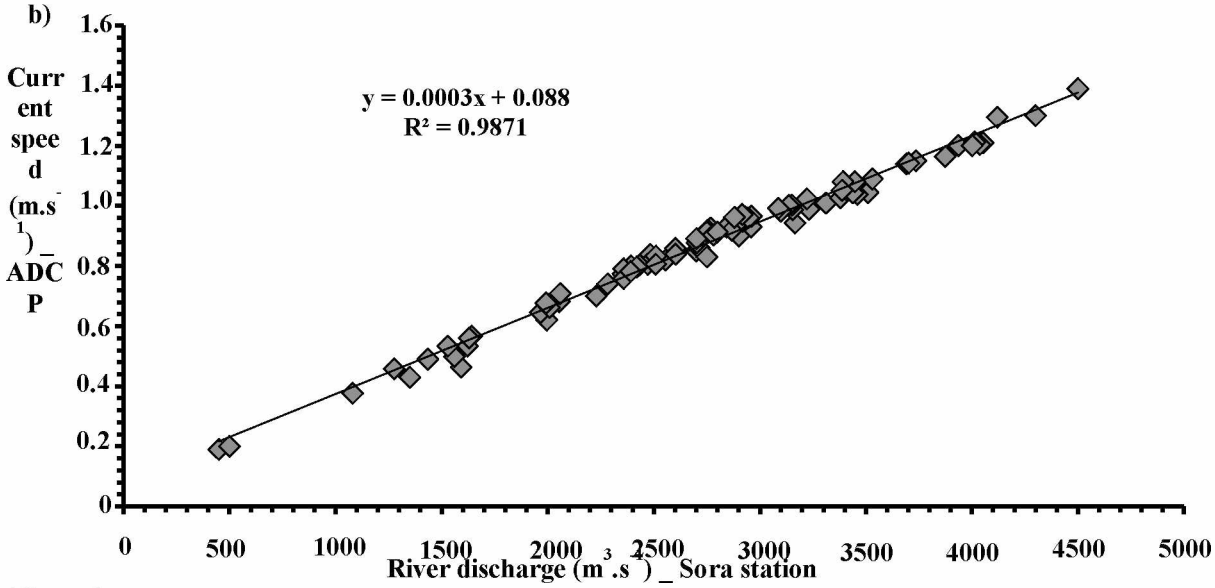
y = 0.0003x + 0.088
R² = 0.9871
Current speed (m.s-1) _ ADCP
River discharge (m3.s-1) _ Sora station

Figure 3.

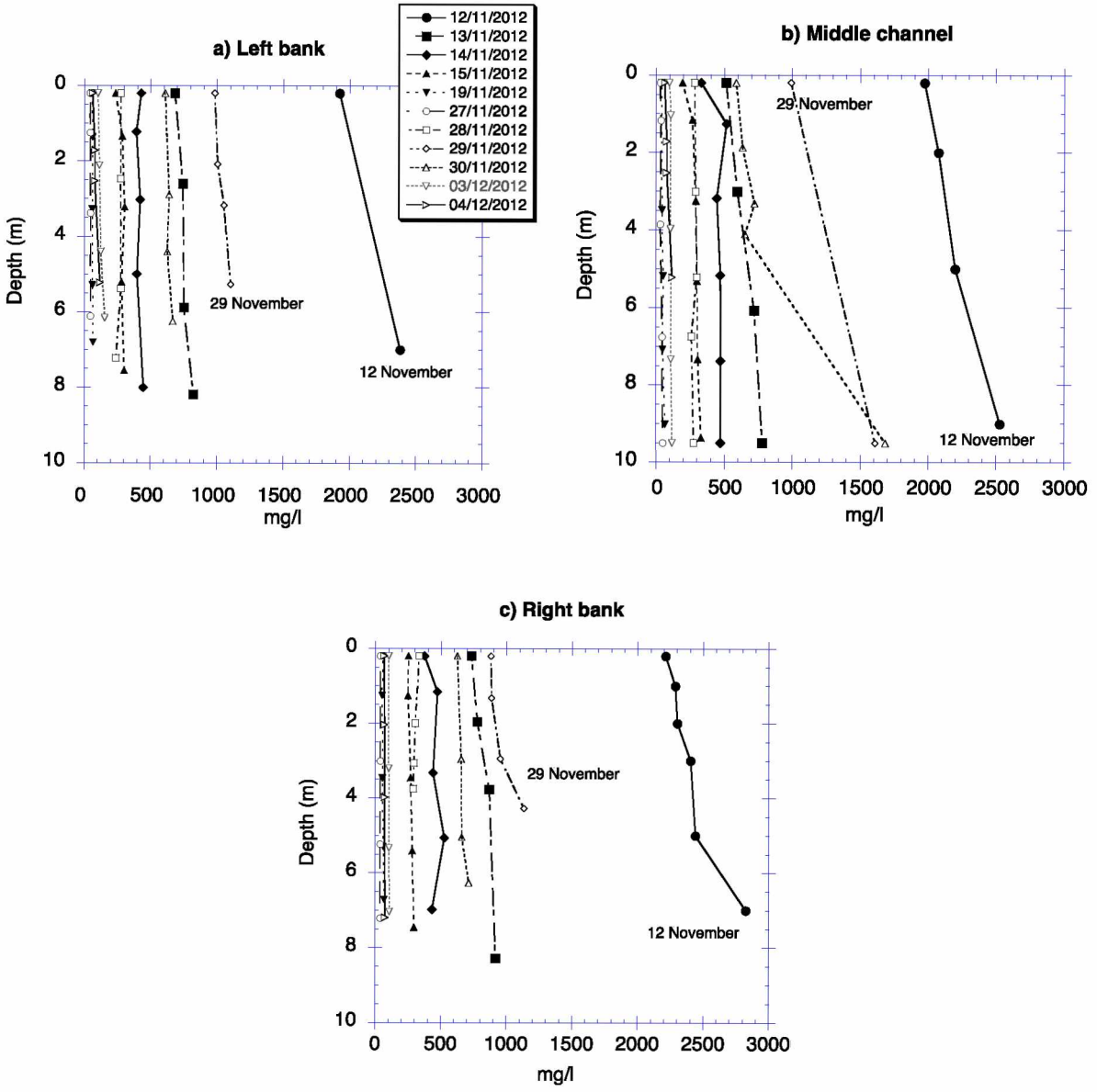
a) Left bank
b) Middle channel
c) Right bank
12/11/2012
13/11/2012
14/11/2012
15/11/2012
19/11/2012
27/11/2012
28/11/2012
29/11/2012
30/11/2012
03/12/2012
04/12/2012
29 November
12 November
Depth (m)
mg/l
0
2
4
6
8
10
0
500
1000
1500
2000
2500
3000

Figure 4.

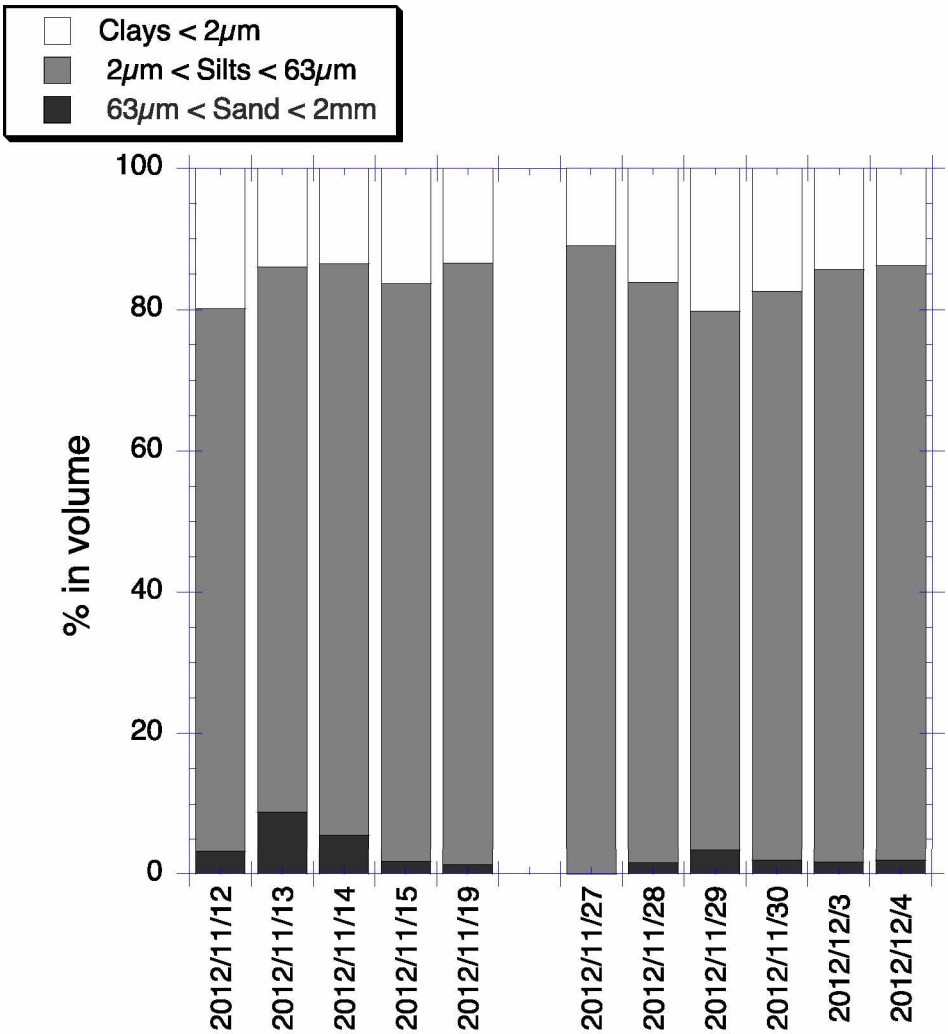
Clays < 2µm
2µm < Silts < 63µm
63µm < Sand < 2mm
% in volume
100
80
60
40
20
0
2012/11/12
2012/11/13
2012/11/14
2012/11/15
2012/11/19
2012/11/27
2012/11/28
2012/11/29
2012/11/30
2012/12/3
2012/12/4

Figure 5.

a). Conversion of backscatter to SSC with water samples

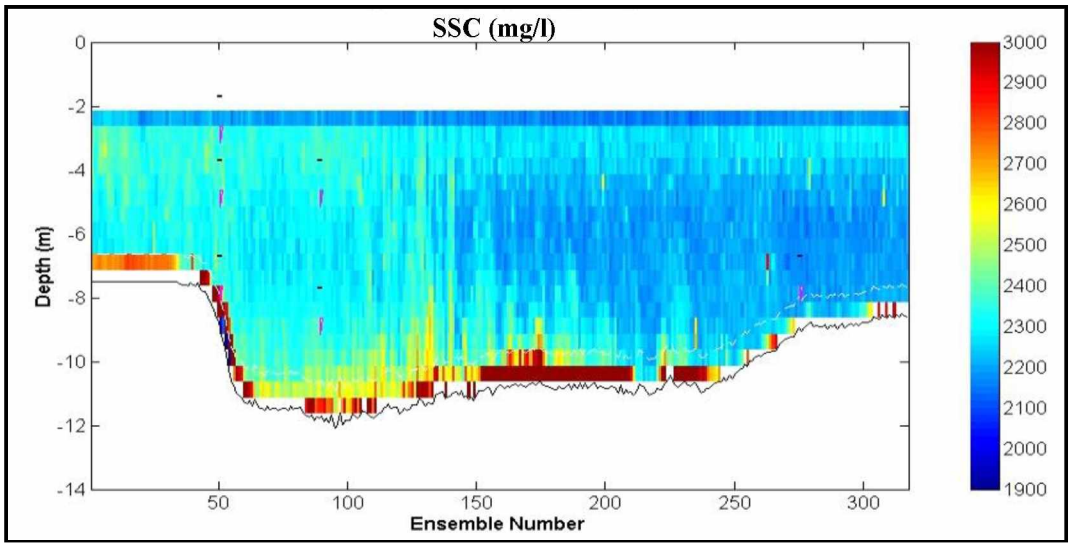

b). Signal correction with grain size distribution

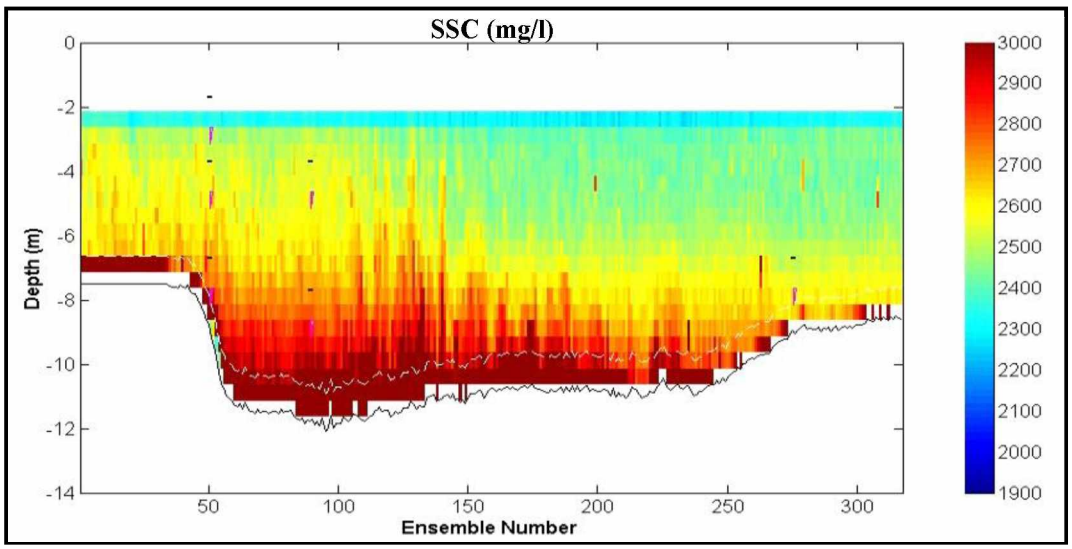

Figure 6

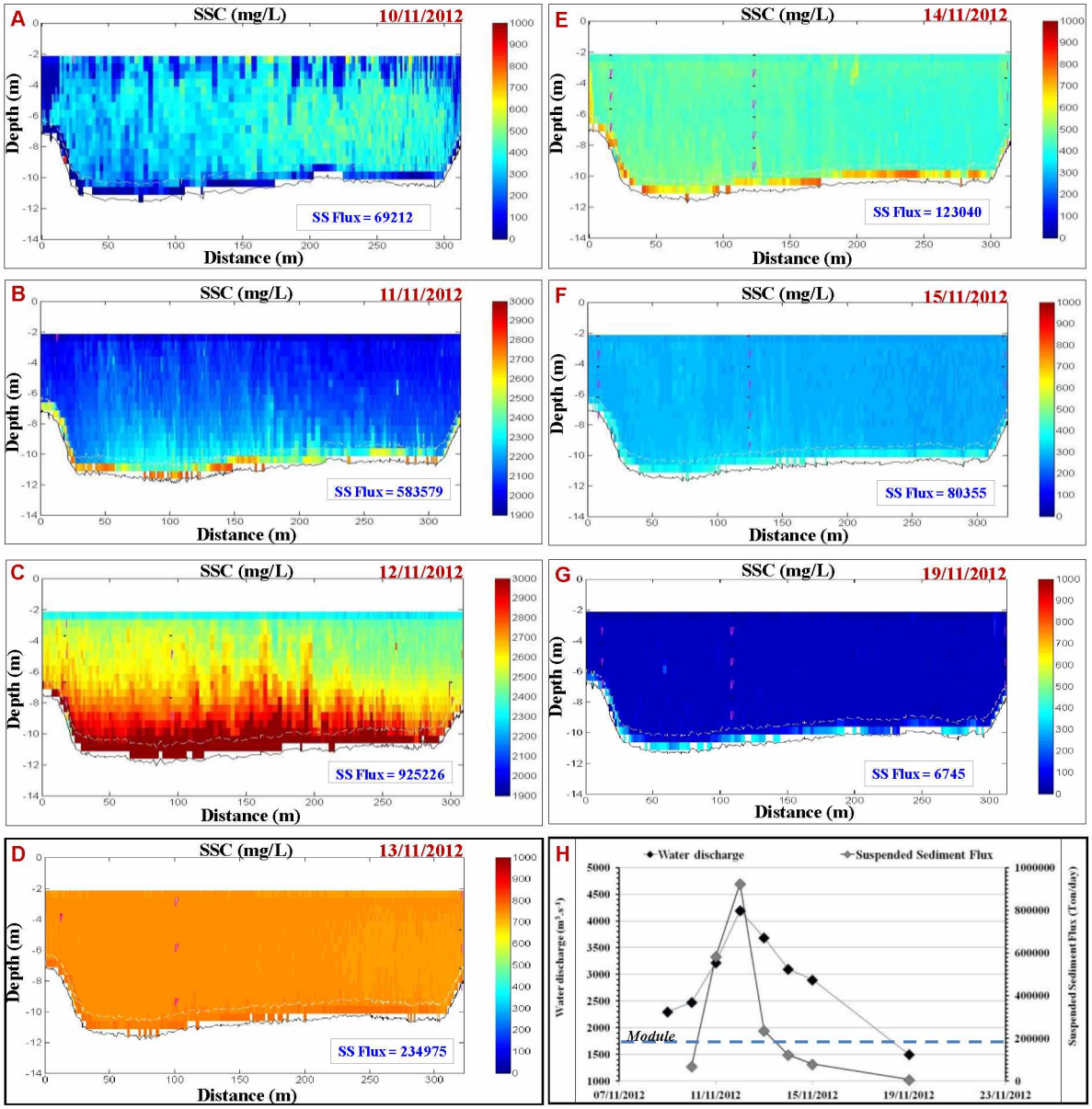
A
SSC (mg/L)
10/11/2012
SS Flux = 69212
E
SSC (mg/L)
14/11/2012
SS Flux = 123040
B
SSC (mg/L)
11/11/2012
SS Flux = 583579
F
SSC (mg/L)
15/11/2012
SS Flux = 80355
C
SSC (mg/L)
12/11/2012
SS Flux = 925226
G
SSC (mg/L)
19/11/2012
SS Flux = 6745
D
SSC (mg/L)
13/11/2012
SS Flux = 234975
Depth (m)
Distance (m)
H
Water discharge
Suspended Sediment Flux
Module
Water discharge (m³.s⁻¹)
Suspended Sediment Flux (Ton/day)
07/11/2012
11/11/2012
15/11/2012
19/11/2012
23/11/2012

Figure 7.

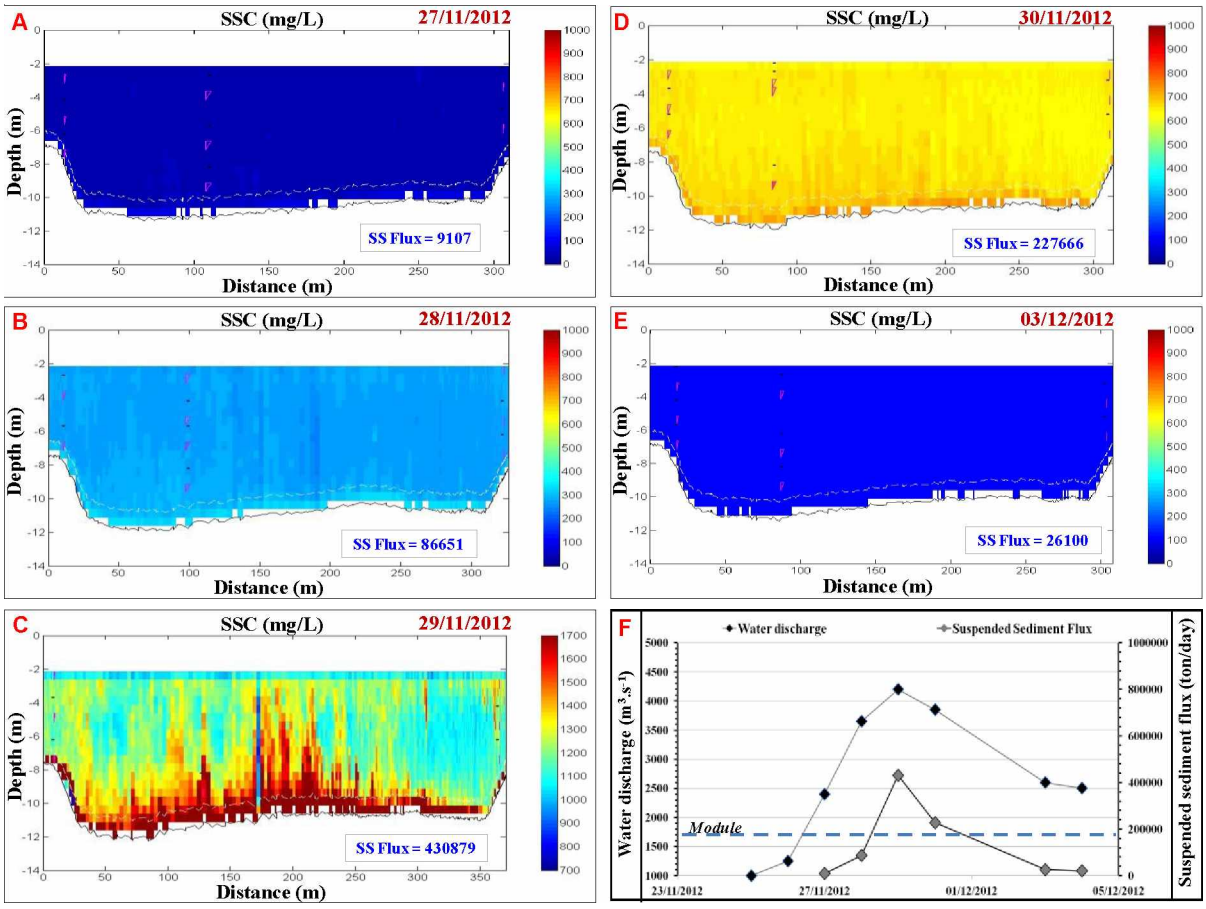
A
SSC (mg/L)
27/11/2012
SS Flux = 9107
B
SSC (mg/L)
28/11/2012
SS Flux = 86651
C
SSC (mg/L)
29/11/2012
SS Flux = 430879
D
SSC (mg/L)
30/11/2012
SS Flux = 227666
E
SSC (mg/L)
03/12/2012
SS Flux = 26100
Depth (m)
Distance (m)
F
Water discharge
Suspended Sediment Flux
Module
Water discharge (m³.s⁻¹)
Suspended sediment flux (ton/day)
23/11/2012
27/11/2012
01/12/2012
05/12/2012

Figure 8.

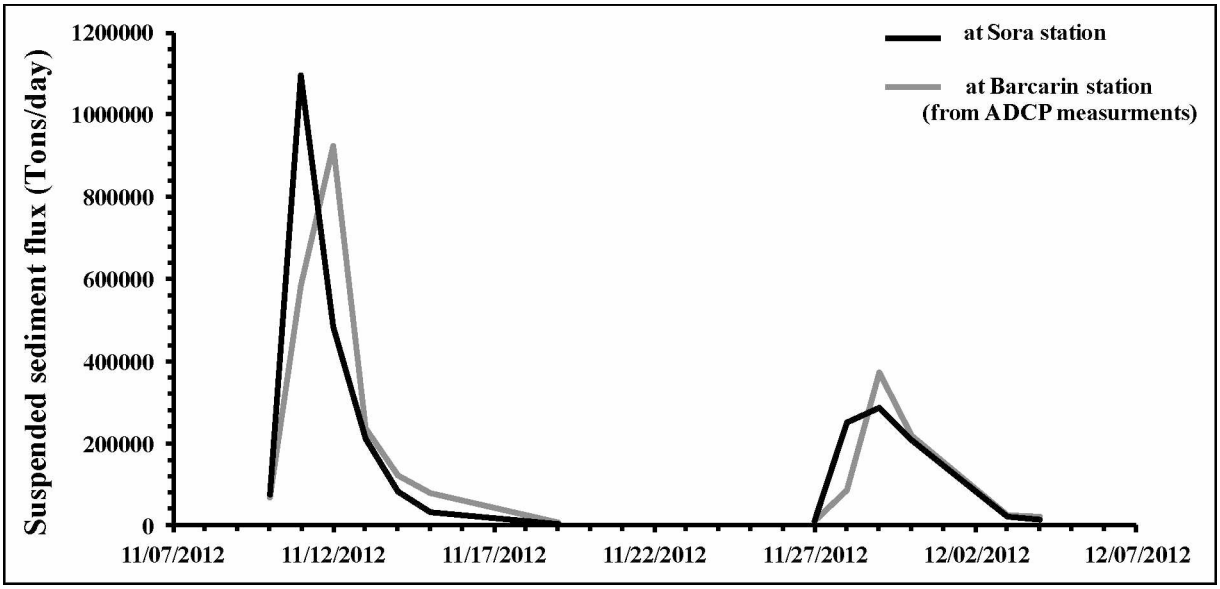
Suspended sediment flux (Tons/day)
1200000
1000000
800000
600000
400000
200000
0
11/07/2012
11/12/2012
11/17/2012
11/22/2012
11/27/2012
12/02/2012
12/07/2012
at Sora station
at Barcarin station
(from ADCP measurments)

Figure 9.